Enhanced microlithography using coated objectives and image duplication

Miklós Erdélyi, Zsolt Bor, Gábor Szabó and Frank K. Tittel*

JATE University, Department of Optics and Quantum Electronics,

H-6720 Szeged, Dóm tér 9, P. O. Box 406, Hungary

*Rice University, ECE Dept. P. O. Box 1892, Houston, TX 77251

ABSTRACT

Two processes were investigated theoretically using both a scalar wave optics model and a microlithography simulation tool (Solid-C). The first method introduces a phase-transmission filter into the exit pupil plane. The results of both the scalar optics calculation (aerial image) and the Solid-C simulation (resist image) show that the final image profile is optimum, when the exit pupil plane filter is divided into two zones with the inner zone having a phase retardation of π rad with respect to the outer one and the ratio of the radii of the zones is 0.3. Using this optimized filter for the fabrication of isolated contact holes, the focus-exposure process window increases significantly, and the depth of focus (DOF) can be enhanced by a factor of 1.5 to 2.

The second technique enhances the DOF of the aerial image by means of a birefringent plate inserted between the projection lens and the wafer. As the shift in focus introduced by the plate strongly depends on the refractive index, two focal points will appear when using a birefringent plate instead of an isotropic plate: the first one is created by the ordinary, and the second one is created by the extraordinary ray. The distance between these images can be controlled by the thickness of the plate. The results of the calculations show that application of a thin but strongly birefringent material is a better candidate than using a slightly birefringent but thick plate, since aberrations proportional to the thickness can cause undesirable effects.

1. INTRODUCTION

In recent years several methods have been proposed and investigated in optical microlithography to improve the quality of final resist images. Since any significant stepper modification implies serious expenses, implementation and compatibility determine the requirements of any new super resolution technique. A new process that requires minimal optical stepper modification is a much more likely candidate than a technically less feasible one, even if the expected resolution and DOF enhancement is less.

Both Incoherent and Coherent Multiple Imaging (IMI and CMI) are well-known processes in optical lithography. The FLEX method increases the DOF significantly using multiple exposures[1,2] . The mask is shifted between the exposures, hence the intensities and not the electric fields are added on the surface of the resist. FLEX is especially effective for the fabrication of contact holes. However, since the mask-lens distance in most steppers is not changeable, FLEX requires an additional, motorized precision positioning system. Coherent multiple imaging, such as Super-FLEX[3,4,5] or pupil plane filtering is technically difficult to implement, since the pupil plane of an optical stepper lens usually cannot be reached unless the lens is disassembled.

The purpose of this paper is the detailed investigation of two techniques that do not require major stepper modifications, but are able to increase the DOF of the aerial image.

M.E.: Email: erdelyim@sol.cc.u-szeged.hu; Fax: 36-62-322529
F.K.T.: Email: fkt@ece.rice.edu; Fax: (713) 524-5237

0277-786X/98/$10.00

2. OPTICAL ENHANCEMENT BY MEANS OF A COATED OBJECTIVE

The theoretical investigation of the resolving power of a coated objective dates back to nearly 50 years[6,7,8]. The problem of coating the objective in order to obtain a diffraction pattern having the smallest central bright spot was studied by John W. Y. Lit in 1971. He pointed out that the diffraction pattern in the focal plane of the lens has the smallest central bright spot when the aperture is divided into two zones, with the inner zone having a phase retardation of π rad with respect to the outer one. The transmission of both parts is 1. It should be noted that "coated objective" is a traditional term, since it actually means an exit pupil plane filter.

2.1 WAVE OPTICS MODEL

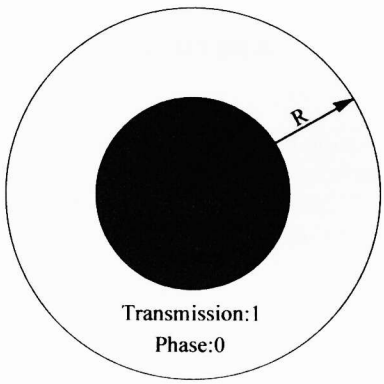

Figure 1. General annulus.

The total complex disturbance $E(P)$ at point P near the focus using a perfect lens and a general annulus shown in Figure 1 is:

$$E(P) = \frac{ikR^2}{f} e^{ik(f-OP)} \left\{ \int_0^1 e^{\frac{1}{2}iu\rho^2} J_0(v\rho)\rho d\rho + (e^{i\pi} - 1)\varepsilon^2 \int_0^1 e^{\frac{1}{2}iu'\rho^2} J_0(v'\rho)\rho d\rho \right\}, \tag{1}$$

where: $u = kR^2 z / f^2$, $v = krR / f$, $k = 2\pi / \lambda$, $r = (x^2 + y^2)^{1/2}$, ρ is the radius vector in the observation surface, ε is the obstruction ratio defined by R'/R, O is the geometrical focus, and f is the focus length.
Equation 1 can be written in terms of the Lommel functions,

$$\int_0^1 e^{\frac{1}{2}iu\rho^2} J_0(v\rho)\rho d\rho = \frac{1}{u} e^{\frac{1}{2}iu} \{U_1(u,v) - iU_2(u,v)\} \tag{2}$$

$$\int_0^1 e^{\frac{1}{2}iu'\rho^2} J_0(v'\rho)\rho d\rho = \frac{1}{u'} e^{\frac{1}{2}iu'} \{U_1(u',v') - iU_2(u',v')\}, \tag{3}$$

where $U_1(u,v)$ and $U_2(u,v)$ are the Lommel functions defined by

$$U_n(u,v) = \sum_{s=0}^{\infty} (-1)^s \left(\frac{u}{v}\right)^{n+2s} J_{n+2s}(v) \quad . \tag{4}$$

The intensity at point P is $I(P)=|E(P)|^2$:

$$I(P)=\frac{k^2R^4}{f^2u^2}\left|e^{\frac{1}{2}iu}(U_1-iU_2)-2\cdot e^{\frac{1}{2}i\varepsilon^2u}(U'_1-iU'_2)\right|^2 . \tag{5}$$

In the geometrical focal plane: u→0 and

$$\lim_{u\to 0}\frac{U_1(u,v)}{u}=\frac{J_1(v)}{v} \tag{6}$$

$$\lim_{u\to 0}\frac{U_2(u,v)}{u}=0, \tag{7}$$

hence

$$I(0,r)=\frac{\pi^2R^4}{\lambda^2f^2}\left[\frac{2J_1(v)}{v}-2\varepsilon^2\frac{2J_1(\varepsilon v)}{\varepsilon v}\right]^2. \tag{8}$$

Along the axis $v=0$

$$U_2(u,0)=1-\cos\frac{1}{2}u, \tag{9}$$

$$U_1(u,0)=\sin\frac{1}{2}u \tag{10}$$

hence

$$I(z,0)=\frac{\pi^2R^4}{f^2\lambda^2}\left[2(1-\varepsilon^2)^2\left(\frac{\sin 1/4u(1-\varepsilon^2)}{1/4u(1-\varepsilon^2)}\right)^2-\left(\frac{\sin 1/4u}{1/4u}\right)^2+2\varepsilon^4\left(\frac{\sin 1/4\varepsilon^2u}{1/4\varepsilon^2u}\right)^2\right]. \tag{11}$$

The above equations were evaluated and depicted graphically by means of a MatCad program. The purpose of the calculations was to find the optimal value of the obstruction ratio. Since the results of the calculations show that the optimized value of the obstruction ratio does not depend on the lens parameters, a simple lens was used with the following parameters: R=5mm; f=25mm; λ=632nm. Figure 4 depicts relative radial and axial scaling to allow an evaluation of the resolution and DOF enhancement.

Figure 2 shows the intensity distribution in the geometrical focal plane when the obstruction ratio changes from 0 to 1. In the case of $\varepsilon = 0$ and $\varepsilon = 1$ the intensity distribution is the well-known Airy pattern. If the obstruction ratio is increased, the intensity of the main central peak begins to decrease and reaches its minimum (0) value when $\varepsilon = 0.7071$. If the value of ε further increases, the intensity of the central peak begins to increase again. It is worth noting here that the intensity of the first diffraction ring grows continuously if ε increases.

Figure 3 depicts the axial intensity distribution related to ε. There is a range of ε where two foci appear. In case of $\varepsilon=0$ and $\varepsilon=1$ the axial intensity distribution is the well-known $(\sin(x)/x)^2$ function. If we use the definition that *DOF* is the axial distance between the central main peak and the first minimum, a coated objective always has a larger *DOF* than an uncoated one, except when $\varepsilon=0.7071$.

From the microlithographic viewpoint, high intensity side lobes cause undesirable interference effects. In what follows, the maximum acceptable intensity of the first diffraction ring was defined as 10% of the central main peak (10% condition).

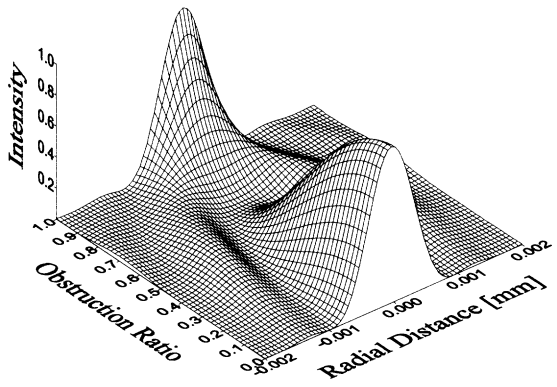

Figure 2. Intensity distribution on the focal plane related to the obstruction ratio.

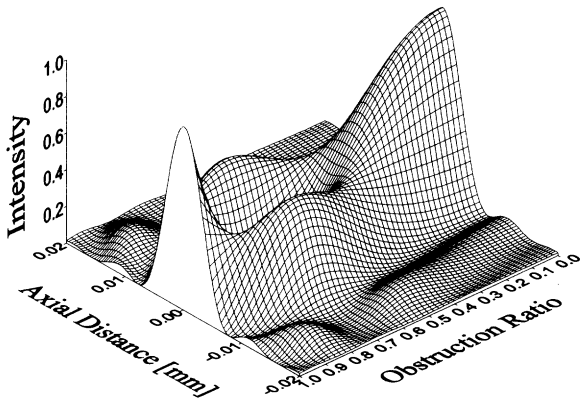

Figure 3. Intensity distribution on the optical axis related to the obstruction ratio.

The 10% condition divides the range of ε into three parts:

Part 1: $0 < \varepsilon < 0.3$
Part 2: $0.3 < \varepsilon < 0.84$
Part 3: $0.84 < \varepsilon < 1$.

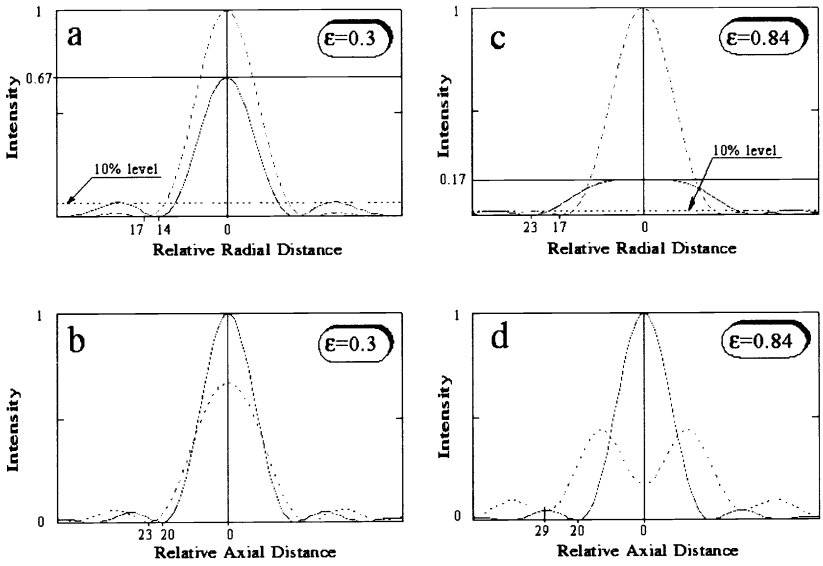

Figure 4. Radial and axial intensity distribution in the two borderline cases.

The intensity of the side lobes is lower than 10% of the central peak in parts 1 and 3. Since the intensity of the first diffracted ring continuously grows if ε increases, it is very interesting that with a relatively high obstruction ratio ($\varepsilon > 0.84$) the 10% condition is still satisfied. This is due to the special topology of the surface; the intensity of the central maximum decreases if ε increases to the value of $\varepsilon = 0.7071$, and the radius of the first diffracted ring decreases continuously. If the value of ε is further increased, the first ring closes ($\varepsilon > 0.7071$) and produces a central peak. The two borderline cases, when the intensity of the first diffraction ring is 10% of the main peak, can be seen in Figure 4. To make the evaluation easier, every figure depicts the original normalized Airy pattern. In case of $\varepsilon = 0.3$ the loss of light is around 33% (Figure 4.a), while in case of $\varepsilon = 0.84$ the loss is around 83% (Figure 4.c).

The *DOF* of a coated objective is always larger than the *DOF* of an uncoated objective, independent of the value of the obstruction ratio; except in one case, when $\varepsilon = 0.7071$, and the intensity in the focal point becomes zero. The *DOF* enhancement in the borderline cases is 15% (Figure 4.b) and 45% (Figure 4.d), respectively. However, the axial intensity distribution in case of $\varepsilon = 0.84$ is not homogeneous.

The resolution power of a coated objective is better than that of an uncoated objective if the obstruction ratio is smaller than 0.7071. (The resolution was defined as the radial distance between the main peak and the first minimum.) Figure 4.a shows a 17% enhancement of resolution. In the other borderline case ($\varepsilon = 0.84 > 0.7071$) the resolution power decreases by 35%.

2.2 SIMULATIONS USING SOLID-C

An optical lithography simulation software (Solid-C) was used to evaluate the optical enhancement applying the previously optimized exit pupil plane filter. During the simulation, the following parameters were used:

- Wavelength: 248 nm
- Power: 50 mJ/cm^{2}s
- Numerical Aperture: 0.5
- Magnification: 5
- Coherence: 0.5
- Flare: 2
- Pupil Shape: Circle
- Image model: Normal
- TAR: Optimized TAR
- Wafer: ST3 Nololac positive
- Underlaying Layer: Optimized ARC
- Substrate: Poly-Silicon

The mask was a simple opaque chrome mask with isolated contacts. The Rayleigh limit of resolution ($CD = 0.61\lambda/NA$) using a stepper lens with parameters defined above is 0.3 μm. Therefore, first the designed *CD* on the wafer was 0.3 μm and the distance between the contacts was 1.5 μm.

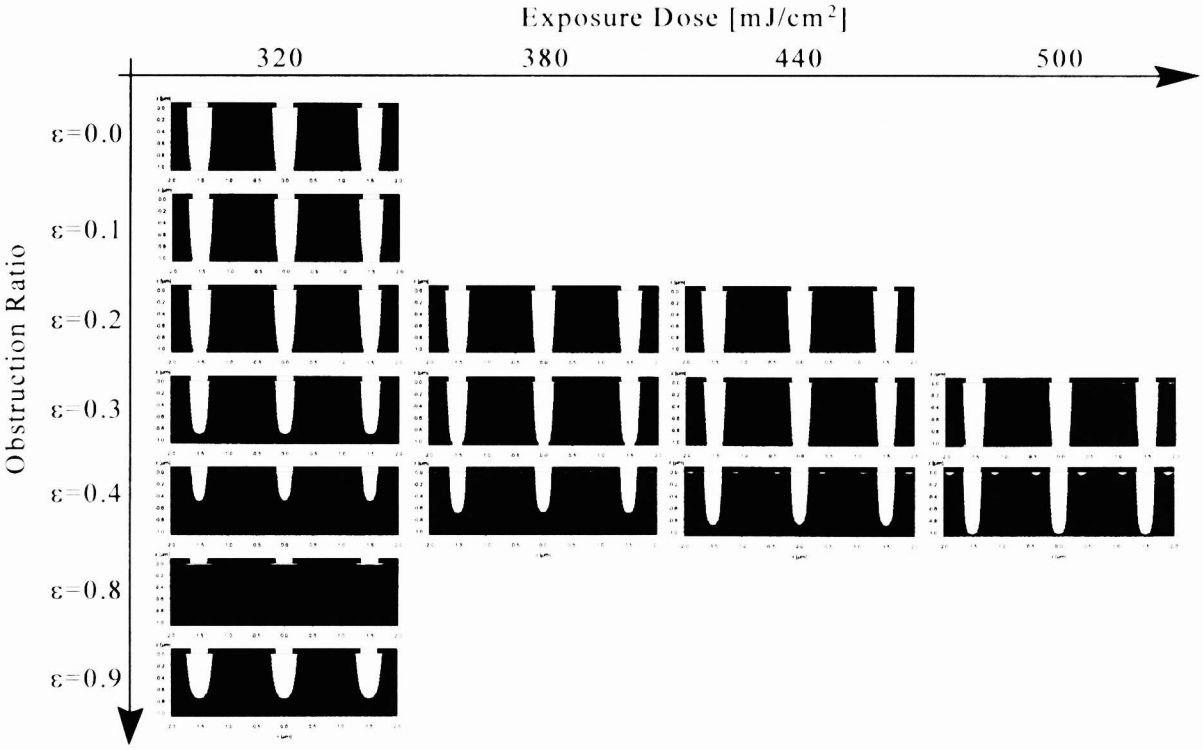

Figure 5. Photoresist profiles with different values of ε and exposure doses.

Since the displayed calculated aerial image does not scale with the exposure dose using Solid-C, the final photoresist profiles were evaluated. The optimization of the process steps[9] between the aerial image and final resist profile calculation (wafer reflection, thin film effects, photochemical processes etc.) is beyond the scope of this paper. During the simulation we used optimized prebuilt process parameters.

Figure 5 depicts the photoresist profile in the focus after exposure using different obstruction ratios and exposure doses. The intensity change with the increasing ε can be seen very clearly. The figure does not show the cases of ε=0.5-0.7, since in this range the intensity is practically zero. The figure does not depict the case of ε=1 either, since the wafer profile is the same when we use a clear, uncoated aperture. Solid-C does not take into account the thickness of the coating. Of course by increasing the exposure dose the profile can be enhanced. The optimum case is around ε=0.3. From the previous part we know that the intensity of the side lobes does not exceed 10% of the main peak. On the other hand, the required exposure dose enhancement (≈1.56) is not critical. In case of ε=0.4 the 1.5 exposure dose enhancement is not enough.

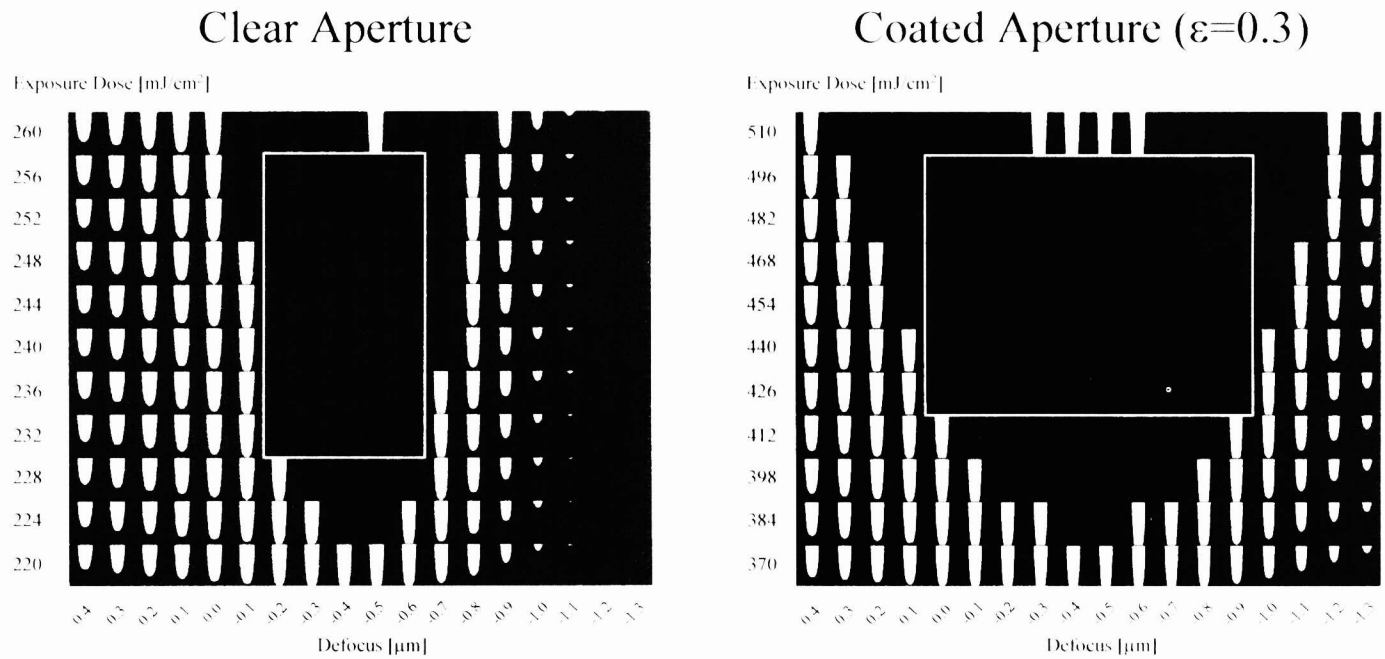

Figure 6. Focus-exposure process windows using uncoated and coated aperture.
The resolution is 0.3 μm.

Figure 6 shows the exposed wafer profile (just the central contact) for different focal positions as a function of the exposure dose using a clear (ε=0) and coated aperture (ε=0.3), respectively. The shaded parts depict the range where the parameters are in the acceptable process tolerances (10% tolerance in CD). The sides of the maximum rectangles inside the focus-exposure process window show the DOF and acceptable exposure dose range.

If a clear uncoated exit pupil is used, the DOF is only 0.5 μm and the useful energy range lies between 230 and 258 mJ/cm^2 (ΔE=28 mJ/cm^2). When using a coated objective, the exposure dose must be increased; the useful energy range is between 419 and 503 mJ/cm^2 (ΔE=84 mJ/cm^2). The increased exposure intensity is almost twice larger than when a clear aperture is used. The exposure dose scales in Figure 6 are not the same! In addition, the DOF increases to 1μm, i.e. becomes twice as large as without the filter.

The efficiency of the exit filter was also studied using a mask with contacts smaller than the Rayleigh limit. Figure 7 depicts the focus-exposure dose process windows for 0.25 μm contact holes. The process window belonging to the 0.25 μm contacts is smaller than when 0.3 μm contacts are exposed. However, exit pupil plane filtering enhances the process window significantly. The useful energy range without the filter is between 354 and 362.4 mJ/cm^2 (ΔE=8.4 mJ/cm^2) while with the

filter it lies between 554 and 594 mJ/cm^2 (ΔE=40 mJ/cm^2). On the other hand, the DOF is 0.6 μm, 1.5 times larger than without the filter.

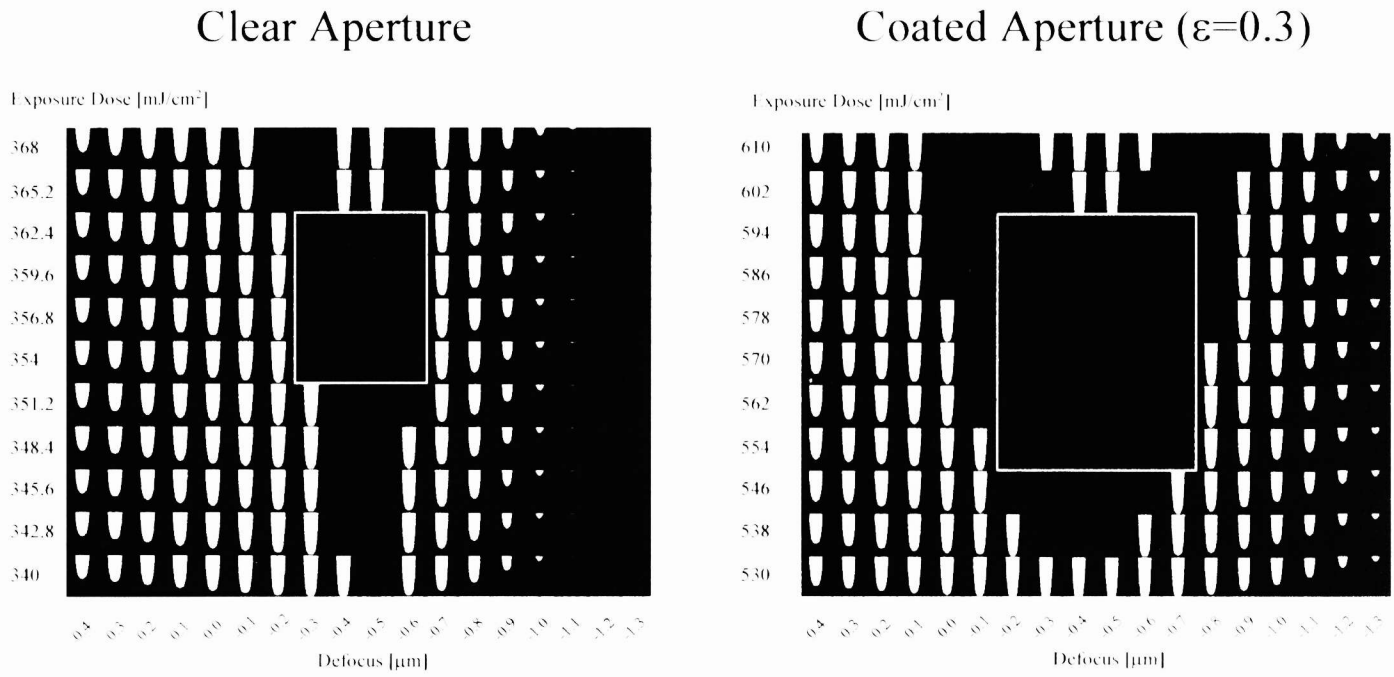

Figure 7. Focus-exposure process windows using uncoated and coated aperture. The resolution is 0.25 μm.

It should be noted that the simulation results and the wave optics model agree. Both calculations show that the optimum obstruction ratio is 0.3. In this case, the focus-exposure process window is enhanced significantly (the DOF increased by a factor of 1.5-2, while the useful energy range by a factor of 3-4), and the intensity of the first diffraction ring is below 10% of the main peak, and the required energy increases by 60-80%. For simulation, we use isolated contacts (the distance between the holes is 5 times of the diameter of the holes), and hence interference effects between the first diffraction rings was not investigated. A study of dense hole and other patterns is the scope of future work.

3. IMAGE DUPLICATION BY MEANS OF A BIREFRINGENT PLATE

The displacement of the focus point when a plane parallel plate is placed behind a lens is a well-known fact. Based on geometrical optics considerations, the shift of focus (Δf) is:

$$\Delta f = d \cdot \left(1 - \frac{\cos(\alpha)}{\sqrt{n^2 - \sin(\alpha)^2}} \right) , \qquad (12)$$

where d is the thickness, n is the refractive index of the plate and α is the incident angle.

As the focus shift depends on the refractive index, we expect that using a birefringent plane parallel plate instead of the isotropic plate, two focal points will appear: the first one is created by the ordinary, and the second one is created by the extraordinary ray (o/e images). We deal with the case when the optical axis is perpendicular to the surface's normal.

The intensity distribution after the birefringent plate in the vicinity of the focal point was calculated using scalar wave optics model[10,11]. The angle dependant phase error introduced by the thin plane-parallel plate is:

$$\phi(\alpha) = k \cdot d(n_2 \cos\beta - n_1 \cos\alpha), \qquad (13)$$

where β is the refractive angle in the plate, n_2 is the refractive index of the plate and n_1 is the refractive index of the environment (we assume that the system is in vacuum, hence n_1=1).

Let us introduce a new variable: $s = \sin\alpha/2$, and let us expand $\phi(s)$ in terms of a power series in s. By means of this new variable, the defocus can be represented by a single term.

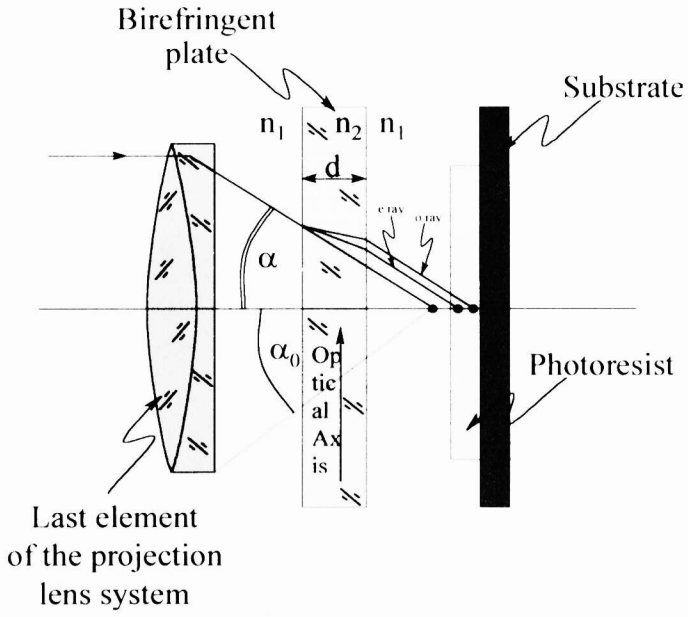

Figure 8. Focusing through a birefringent plate.

$$\phi(s) = k \cdot d(n_2 - n_1)\left\{1 + \frac{2n_1}{n_2}s^2 + 2(n_2 + n_1)\frac{n_1^2}{n_2^3}s^4 + 4(n_2 + n_1)\frac{n_1^4}{n_2^5}s^6 + \ldots\right\} \qquad (14)$$

The term in s^2 represents the defocus introduced by the slab, while the term in s^4 represents the primary spherical aberration. Using the scalar theory the intensity in the focal region is:

$$I(u,v) = \left| \int_0^{\alpha_0} \sqrt{\cos\alpha} \cdot e^{i\phi(\alpha)} J_0\left(\frac{v\sin\alpha}{\sin\alpha_0}\right) \cdot e^{-\frac{1}{2}iu\frac{\sin^2\left(\frac{\alpha}{2}\right)}{\sin^2\left(\frac{\alpha_0}{2}\right)}} \cdot \sin\alpha \cdot d\alpha \right|^2, \qquad (15)$$

where $u = 4kz\sin^2(\alpha_0/2)$, $v = kr\sin\alpha_0$, and α_0 is the semi-angle of convergence (see Figure 8).

Using the new variable the intensity distribution on the optical axis is:

$$I(u) = \left| \int_0^{\sin\frac{\alpha_0}{2}} B(s) \cdot P(s) \cdot e^{-\frac{1}{2}iu\frac{s^2}{\sin^2\frac{\alpha_0}{2}}} sds \right|^2 \qquad (16)$$

where $B(s) = \{4(2s^2 - 1)\}^{1/4}$ and $P(s) = e^{i\phi(s)}$ is the wavefront aberration function. During the calculation we assumed that the extraordinary refractive index is constant and does not depend on the direction of the ray. We have two reasons for using this simplification. On the one hand we use only part of the refractive index ellipsoid which is determined by the numerical aperture of the projection lens. In case of NA=0.3 (α_0=18°) the maximum refractive index difference inside the illuminated cone is 0.0012 for MgF_2 and 0.014 for calcite, which is smaller than 10% of the difference between the ordinary and extraordinary refractive indexes for both cases. On the other hand, distortions introduced by the non-cylindrical symmetry of the system can also be addressed, if instead of a single "thick" slab, we apply a slab containing several plates, for which the optical axes are rotated against each other.

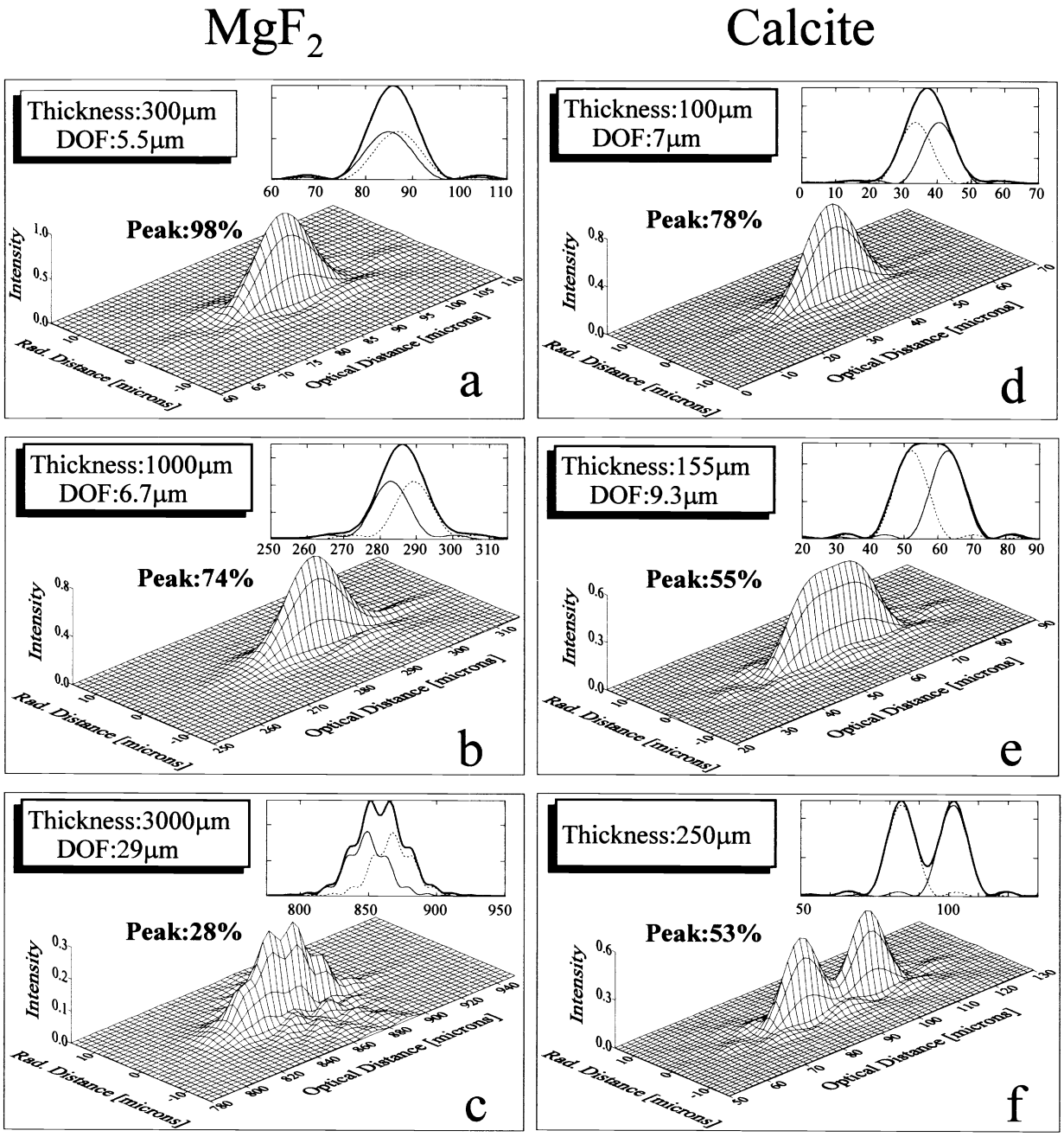

Figure 9. Calculated intensity distribution in the vicinity of the focus point using a birefringent slab inserted behind the lens.

Figure 9 shows the normalized intensity distributions for MgF_2 and calcite slabs using different plate thickness. The numbers adjacent to the peaks display the intensity maxima comparing with the case when no birefringent plate is used and the intensity maximum is 1. The insets depict the 2d intensity distribution on the optical axis. The solid thin lines show the images created by the ordinary rays, the thin dashed lines show the images created by the extraordinary rays, while the thick solid lines depict the total intensity distributions. Since MgF_2 is a positive uniaxial crystal ($n_o<n_e$), the image created by the ordinary ray precedes the image generated by the extraordinary ray. Calcite is a negative uniaxial crystal, hence the order of the o/e images are exchanged. The refractive index difference between the ordinary and the extraordinary rays significantly determines the final image profile. Calcite is a strongly birefringent material (n_o=1.656 n_e=1.485 dn=0.171), hence a thin, almost 155 μm plate is sufficient. In Figure 9.e the separation of the o/e images almost equals their DOF, hence the DOF of

the final image is twice as large as the separated images. Using a thinner plate the o/e images came closer to each other, hence the DOF enhancement is not significant. In case of a thick slab the o/e images are separated and DOF enhancement cannot be obtained.

MgF_2 is a slightly birefringent material (n_o=1.378 n_e=1.39 dn=0.012), therefore a thicker plate is necessary to reach the same effect. Figures 9.a,b,c show the intensity distributions using MgF_2 plates with different thickness. Since a thick slab beyond the projection lens causes undesirable aberration effects (see Figure 9.c), the intensity distributions are not as smooth as they were using calcite plate. The optimum thickness of the MgF_2 plate was around 1000μm (see Figure 9.b). Hence the application of a thin but strongly birefringent material is a better candidate than that of a slightly birefringent but thick plate, since aberrations proportional to the thickness of the plate become insignificant.

Since a birefringent plate located between the projection lens and the wafer cannot be defined in the present microlithography simulation tools, we plan to evaluate the process experimentally.

4. CONCLUSIONS

Two processes were investigated theoretically from the microlithographic point of view to increase the DOF of the aerial image.

Both aerial image calculations (based on scalar wave optics model) and microlithographic simulations (using Solid-C) showed that an appropriately defined exit plane filter is able to enhance DOF by a factor of 1.5 to 2. The focus-exposure process window becomes significantly larger, even if the designed feature size on the resist is below the theoretical Rayleigh limit.

A birefringent plate inserted between the projection lens and the wafer shifts the foci created by the ordinary and the extraordinary rays to different amounts. The distance between these images can be controlled by the thickness of the plate, and strongly depends on the refractive index. Since aberrations proportional to the thickness of the plate cause undesirable distortions, the application of a thin but strongly birefringent material is a better candidate than using a slightly birefringent but thick plate.

5. ACKNOWLEDGEMENT

This research was supported in part by OTKA Foundation of the Hungarian Academy of Sciences (T020910) and the Texas Instruments Inc. University Research program.

6. REFERENCES

1. H. Fukuda, N. Hasegawa, T. Tanaka and T. Hayashida, "A New Method for Enhancing Focus Latitude in Optical Lithography: FLEX", *IEEE Electron Device Letters*, **EDL-8(4),** pp. 179-180, 1987.
2. H. Fukuda, N. Hasegawa and S. Okazaki, "Improvement of defocus tolerance in a half-micron optical lithography by the focus latitude enhancement exposure method: Simulation and experiment", *J. Vac. Sci. Technol. B*, **7(4)**, pp. 667-674, 1989.
3. H. Fukuda, "Axial Image Superposing (Super-FLEX) Effect Using the Mask Modulation Method for Optical Lithography", *Jpn. J. Appl. Phys*, **30(11B),** pp. 3037-3042, 1991.
4. H. Fukuda, T. Terasawa and S.Okazaki, "Spatial filtering for depth of focus and resolution enhancement in optical lithography", *J. Vac. Sci. Technol. B*, **9(6),** pp. 3113-3116, 1991.
5. Handbook of Microlithography, Micromachining, and Microfabrication, Volume 1: Microlithography, Editor: P. Rai-Choudhury, SPIE Optical Engineering Press, pp. 73, 1997.
6. H. Osterberg and J. E. Wilkins, Jr., "The Resolving Power of a Coated Objective", *J. Opt. Soc. Am.,* **39(7),** pp. 553-557, 1949.
7. J. E. Wilkins, Jr., "The Resolving Power of a Coated Objective II", *J. Opt. Soc. Am.,* **40(4),** pp. 222-224, 1950.
8. J. W. Y. Lit, "Effects of a Half-Wave filter in a Portion of the Aperture of a Perfect Lens", *J. Opt. Soc. Am.,* **61(3),** pp. 297-302, 1971.
9. T. Brunner, "Pushing the limits of lithography for IC production", IEDM'97, Washington, DC, December 7-10, 1997.

10. C. J. R. Sheppard and H. J. Matthews, "Imaging in high-aperture optical systems", *J. Opt. Soc. Am. A*, **4(8)**, pp. 1354-1360, 1987.
11. C. J. R. Shepperd and C. J. Cogswell, "Effects of aberrating layers and tube length on confocal imaging properties", *Optik*, **87(1)**, pp. 34-38, 1991.